

Mixing in an enclosed microfluidic chamber through moving boundary motions

Chengpeng Yang¹ · Dinglong Hu¹ · Baoce Sun¹ · Xin Cui¹ · Qian Zhu¹ · Raymond H. W. Lam¹

Received: 12 January 2015 / Accepted: 11 May 2015 / Published online: 20 May 2015
© Springer-Verlag Berlin Heidelberg 2015

Abstract Mixing in enclosed culture micro-chambers is an important criterion on achieving the long-term cell growth with more consistent characteristics spatially distributed in the microfluidic environments. Here, we report a microfluidic mixer composed of multiple deformable membranes to drive circulation flows within the culture region in a peristaltic manner. This mechanically driven mixing scheme has the advantages over many others existing mixing schemes by inducing negligible shear stress over cells without side effects to the viability and growth characteristics. The membrane movements can induce moving boundary motions of the liquid volume contained in the culture chamber. The flow characteristics such as the velocity profile and shear stress are investigated by lumped-element modeling and computational simulations. Both experiments and simulations are performed to show the effectiveness of the mixing of both soluble substances and sub-microscale particles, including bacteria. The mixing performance under different operation parameters (e.g., membrane size and membrane switching time) is also investigated for the optimized operation. Further, the dental bacteria *Streptococcus mutans* are cultured for 2 days to demonstrate that the reported mixing scheme can generate a more even distribution of growth, which may be further applied for a

uniform dental biofilm development in vitro for the related biofilm research. Additionally, this micro-mixer is highly compatible with the widely used soft lithography technique, and hence, it can be directly integrated with general microfluidic devices for extended biomedical diagnosis and bio-sample processing applications.

1 Introduction

In the past decades, microfluidics has been widely applied in chemical and biological applications in the microscales. For instance, microfluidics plays an important role in the long-term cell cultivation and analyses as micro-bioreactors, in which cells may grow and react with selected reagents for drug screening and discovery purposes (Materne et al. 2013; Wu et al. 2008). To maintain the long-term cell viability in the micro-bioreactors, fresh culture media should be regularly perfused into the incubation micro-chambers to refresh nutrients and growth factors. However, this essential process may generate gradients of soluble factors in the incubation region, i.e., with higher concentrations of nutrients and growth factors in the inlet, and thereby cells near the inlet may then grow faster than those in the rest of the chamber region. In the worst case, cell clusters near the inlet may eventually clog the chamber entrance. Therefore, it is important to develop a micro-mixer within an enclosed culture region in order to avoid the mentioned hurdles (e.g., inlet clogging and growth inconsistency) for the long-term cell incubation and analysis applications using microfluidics.

In recent years, many micro-mixers have been developed to achieve more rapid mixing (Capretto et al. 2011; Lee et al. 2011a; Mansur et al. 2008; Nguyen and Wu 2005). These mixers can be briefly categorized into two

Chengpeng Yang and Dinglong Hu have contributed equally.

Electronic supplementary material The online version of this article (doi:10.1007/s10404-015-1596-y) contains supplementary material, which is available to authorized users.

✉ Raymond H. W. Lam
rhwlam@cityu.edu.hk

¹ Department of Mechanical and Biomedical Engineering, City University of Hong Kong, Kowloon Tong, Hong Kong

major groups: the ‘active’ mixers and ‘passive’ mixers for the designs with and without an additional actuator/energy source for the mixing enhancement, accordingly. For the passive mixers, Fu et al. (2014) combined a nozzle and a double-heart chamber with a Y-shaped injection channel. Due to the symmetrical rotating vortex structures, a significant perturbation of the species streams is induced to make more efficient mixing. Tofteberg et al. (2010) reported a lamination mixer with a planar lid on the top of a structured channel. With this structure, flows are made with a 90° rotation between each recombination and splitting. Abbas et al. (2013) developed a continuous-flow micro-mixer based on the channel deflection. Further by generating a chaotic advection using the channel deflection, the mixing efficiency was enhanced significantly. Ansari et al. (2010) designed a passive micro-mixer by splitting the main channel into two sub-channels with different widths. Due to the different flow rates in the sub-channels, unbalanced molecular collisions were created every time when two fluid streams combined. This kind of channel mixers (e.g., the T- or Y-shaped micro-mixers) could only operate with a continuous flow, where detached cells from clusters were removed with the flow. However, the continuous flow condition may not match the required microenvironments for some long-term cell analyses applications such as the biofilm development on tooth or bond surfaces, on which the liquids are static or nearly static.

Micro-mixers functioning inside enclosed microfluidic regions often require complex fabrication, integration and operation (Lin et al. 2007; Zhu and Kim 1998), limiting their practical applications. Typically, these mixers are ‘active’ mixers requiring additional flow induction. The commonly used actuating sources are the electric field (Park and Wereley 2013; Yan et al. 2009) and the magnetic field (Peng et al. 2011; West et al. 2002). Yet, the extra electromagnetic fields may cause direct effects to the cell behaviors and viability, due to factors such as the abundant ions in the growth media and the ion channels over cell membranes. For example, the electric field would enhance the growth of human keratinocyte cells (Vianale et al. 2008), and an electromagnetic field (frequency: 60 Hz) could alter the activity of ornithine decarboxylase in human lymphoma cells and mouse myeloma cells (Byus et al. 1987). Kim et al. (2009) demonstrated a thermal technique by alternating the actuations of two heaters to induce natural convection in the micro-chamber to enhance the mixing rate. This technique should not be applicable in long-term cell applications as the cell growth is very sensitive to the microenvironmental temperature fluctuations. Alternatively, mechanical flow actuation seems to be a more feasible approach. For example, Lee et al. (2011b) worked on a micro-mixer composed of three interconnected deformable growth chambers. The corresponding mixing was achieved

through deflections of the PDMS membranes in a peristaltic manner. While highly functional, it was very challenging to integrate the components into general micro-bioreactors since each culture region was split into three deformable chambers. Hsiung et al. (2007) and Koh and Marcos (2015) demonstrated mixers utilizing moving membrane structures, activated pneumatically by the external air pressure. The mixing efficiency was reasonably good, but cells could be flushed away by the continuous, and hence, the long-term cell culture application was challenging. Xia et al. (2014) utilized a micro-oscillator to generate oscillatory flows and further the induced flow segmentation in order to enhance mixing efficiency. Fu et al. (2013) proposed to apply the pressure disturbances, functioning as the chaotic vortex micro-mixer. Lin et al. (2014) proposed a bubble-driven mixer by driving an air flow through a wooden diffuser to generate bubbles to mix the fluids. However, the gaseous contents in the bubbles could change the culture environment by altering the concentration of dissolved oxygen and carbon dioxide. The piezoelectric micro-mixers were developed to exert a directed physical oscillation at the ultrasound frequencies on the fluid body (Nguyen and Wu 2005). Liu et al. (2002) and Marcos et al. (2014) developed a mixing technique based on the principle of cavitation micro-streaming and bubble-induced acoustic micro-streaming. Nevertheless, an excessive power level of the generated ultrasonic wave may lead to physical damages on the cells. Jang et al. (2007) employed a piezoceramic/silicon diaphragm to generate acoustic streaming to homogenize mixing solution by rapidly switching the resonant frequencies, but the ultrasound caused significant effects on the cell growth (Pitt and Ross 2003). Altogether, there is still a demand for the design of a microfluidic mixer, which can be integrated into high-throughput micro-bioreactors and induces only negligible effects on the growth of individual cells, biofilms or tissues.

Here, we introduce a microfluidic mixer operating in a closed liquid volume, consisting of six deformable membranes, located around the outer area of the ceiling of a cylindrical micro-chamber. The membranes have been grouped as two three-membrane peristaltic flow drivers, in which each membrane was driven by an external computer-controlled air pressure. We may consider the membrane movements as moving boundary motions of the culture chamber, in order to generate circulation flows within the chamber to enhance mixing. We have run simulations to investigate the corresponding flow characteristics. We have also conducted experiments for further verification and quantification of the mixing performance. Dental bacteria named *Streptococcus mutans* have been cultured in a micro-chamber, in order to demonstrate improvements of cell growth with the assist of the reported mixing scheme.

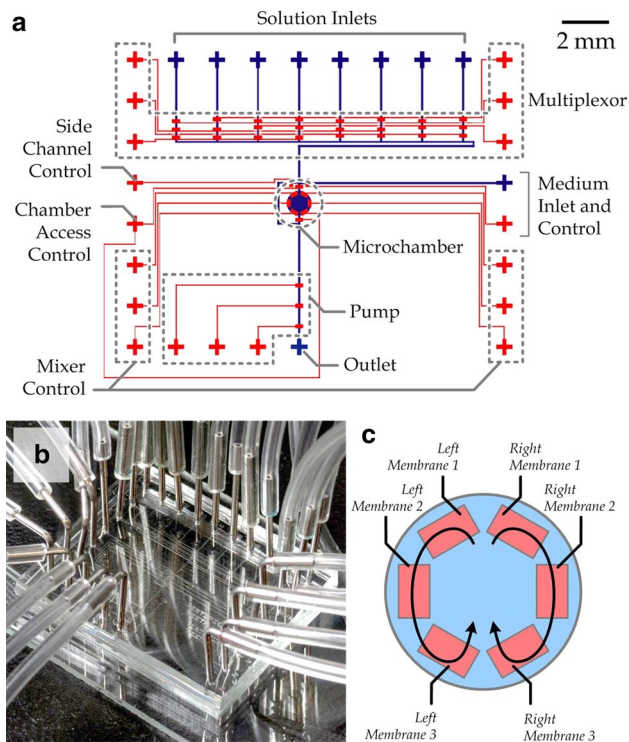


Fig. 1 **a** Layout of a microfluidic peristaltic mixer. The control-channel layer (red) was fabricated overhead the flow-channel layer (blue). The micro-chamber included a circular well (with an additional depth of 50 μm) as its bottom part. **b** An assembled fabricated device connected with tubing for liquid and gas pressure connections. **c** Schematic view of the membranes. The basic peristaltic mixing operation was a recurrent actuation of both sides (left and right) of the membranes (1, 2 and 3) (color figure online)

2 Methods

2.1 Device fabrication

The microfluidic mixer included mainly four layers of microstructures: the control channels, the flow channels, the chambers and a glass substrate (located from top to bottom). The design layout is shown in Fig. 1a. The microfabrication was based on multilayer soft lithography (Unger et al. 2000) (the more detailed procedures are described in *Supplemental Information* and Fig. S1). A fabricated device is shown in Fig. 1b.

2.2 Simulation for flow profiles

We performed computational studies to validate and analyze liquid velocity and pressure profiles generated by the mixer operation. We first applied a lump-element model to compute the membrane deflections during the mixing operations. These estimated deflections and velocities of the membranes were then imposed as moving boundaries and

boundary fluxes of the micro-chamber, respectively. Then, we used commercial simulation software (COMSOL 4.3b, COMSOL Inc., Burlington, MA, USA) to compute the transient flow profiles in the three-dimensional finite-element chamber model. We adopted the laminar flow model instead of solving the full form of Navier–Stokes equations to reduce the computational cost. In fact, the flows can be considered as laminar due to the low Reynolds number ($Re \ll 1$), calculated as described later in flow characteristics. Water (density: 10^3 kg/m^3 ; viscosity: $10^{-5} \text{ cm}^2/\text{s}$) was set as the flowing liquid in the chamber. The purpose of these simulations was to obtain the repeating flow profiles during mixing. In practice, with the zero-velocity initial conditions, simulations were implemented for multiple mixing cycles (typically seven cycles should be sufficient) until the stabilized repeating profiles were obtained. The resultant flow profiles were then used for the following simulations to obtain the transient concentration profiles of both soluble molecules and particles.

2.3 Experiments for mixing characterization

We applied the microfluidic device to mix color dye (McCormick) and fluorescent beads (Cat# FP-0545-2, carboxyl fluorescent light yellow particles, Spherotech, Inc., Lake Forest, IL) to characterize the mixing for soluble molecules and particles (with diameters bigger than 100 nm including bacteria). The bead samples were diluted in 5 % pluronics (Sigma) at a concentration of 0.01 % w/v in order to prevent the adhesion of beads on the chamber walls. In the experiments, we first filled the chamber and channels with water. The selected samples with $\sim 20\%$ of the chamber volume were injected to the chamber through one of the solution inlets. We then captured videos under a fluorescence microscope during the mixing operations of different mixing parameters for further analyses.

2.4 Image analysis

We customized MATLAB scripts (version 8.2, MathWorks, Novi, MI, USA) to quantitatively analyze the mixing performance during mixing based on intensity changes in a micro-chamber. Briefly, we applied image processing on the snapshots at different time points during the mixing operations. We calculated the normalized standard deviations (SD) (Voth et al. 2003) of the snapshots in the chamber region, with the value at the beginning of mixing to be ‘1’ and at the stabilized status to be ‘0.’

2.5 Device preparation for cell culture

To prepare for cell culture experiments, each microfluidic mixer was first sterilized by baking at 100 $^\circ\text{C}$ for >10 h

and UV exposure for >2 h. All control channels and flow regions were initially primed with pressurized DI water with an upstream pressure of ~20.7 kPa. Culture media, distilled water and phosphate-buffered saline (PBS) were then inserted into the medium inlet, and solution inlets one and two, respectively. We placed the mixer on a microscope fitted with an enclosed temperature-controlled shield to provide a stable operating temperature of 37 °C. We then inserted the *S. mutans* bacteria sample (ATCC 25175, ~10⁴ cells/ml) to fill up the micro-chamber using the peristaltic micro-pump lying along the outlet channel of the device. Afterward, we isolated the bacteria by closing the valves at the chamber entrance and exit and incubate for 30 min, to achieve the initial cell attachment.

3 Results and discussion

3.1 Mixer design and basic operation

We have developed a microfluidic peristaltic mixer composed of six micro-membranes fabricated around the ceiling of a micro-chamber. The layout of a proof-of-concept device, which contained a layer of control channels overhead the flow-channel layer, is shown in Fig. 1a. As described in Fig. 1c, the six micro-membranes were grouped as a pair of three-membrane flow drivers working simultaneously with a repeating peristaltic sequence of pressurization of the three membranes: *Membrane 1*, *Membrane 2* and *Membrane 3* in the *left* or *right* side of the chamber. The pressurization was achieved by connecting the inlet control channel for each membrane to a compressed-air source to drive the membrane deflection. While the micro-chamber (diameter: 1 mm; height: 80 μm) was closed by the entrance and exit valves, peristaltic actuation cycles were continuously applied to each three-membrane flow driver. Each mixing cycle contained three pressurization steps: step 1 with *Membrane 1* on and *Membrane 2* and *Membrane 3* off; step 2 with *Membrane 2* on, and *Membrane 1* and *Membrane 3* off; and step 3 with *Membrane 3* on, and *Membrane 1* and *Membrane 2* off. Accordingly, the mixing operation generated two symmetrical flow circulations inside the chamber (indicated with *arrows*).

As mentioned, micro-valves were fabricated at the entrance and exit of the micro-chamber to control for the liquid accessibility. A side channel was located beside the culture chamber such that liquids could flow bypass the micro-chamber. Additionally, there existed a medium channel for injections of fresh culture media on one side of the chamber (*right* in Fig. 1a). A microfluidic peristaltic pump which consisted of three valves was fabricated downstream of the micro-chamber to drive liquid flows from the medium channel, the buffer solution channel, or one of

the eight inlet channels controlled by a microfluidic multiplexer. The eight solution inlets were designed as reserves for potential cell research applications, such as buffer solutions (e.g., PBS), growth factors, supplementary biochemical stimuli for cell responses, and reagents for analyses of cell characteristics.

3.2 Lumped-element model of membrane deflection

To reduce the computational cost and complexity, we decomposed the simulation into three major sub-tasks: (1) determination of moving boundaries of the micro-chamber using a lumped-element model for the membrane dynamics, (2) simulation of the flow velocities in the chamber using the computed moving boundaries and (3) calculation of transient distributions of solutions and particles based on the simulated velocity profiles.

To implement the first sub-task, we simplified the model by considering the physical symmetry of the chamber geometry and operation and taking only a half chamber with the three moving membranes shown in Fig. 2a. Major effects of the membrane dynamics should be the membrane stiffness and the fluidic resistances along the connecting control channels prefilled with water. Here we represented the integrative effects by the equivalent electrical circuit composed of lumped elements. Considering the analogy of constitutive relations in mechanical and electrical domains, we expressed the flow rates as electrical currents and the hydraulic pressures as voltages. Hence, the fluidic resistances along three control channels were represented by electrical resistors (R_1 , R_2 and R_3), and the mechanical stiffnesses of the membranes were equivalent to capacitors (C_1 , C_2 and C_3). R_1 , R_2 and R_3 had identical flowing liquid (water) filled with the same length and channel dimensions, and hence, they were equal to the value R (Senturia 2001),

$$R = \frac{12\mu L_C}{W_C H_C^3} \left/ \left\{ 1 - \frac{192H_C}{\pi^5 W_C} \sum_{n=0}^{\infty} \frac{\tanh[(2n+1)\pi W_C/2H_C]}{(2n+1)^5} \right\} \right. \quad (1)$$

where μ is the viscosity of fluid along channel and L_C , W_C and H_C are the length, width and height of the water sections filled in the channels, respectively. Further, we estimated the membrane stiffness (Timoshenko et al. 1959) as the same value C , due to the same membrane material (PDMS) and dimensions (the calculation is described in *Supplemental Information*):

$$C = \sum_{m=1,3,\dots} \sum_{n=1,3,\dots} \frac{768L_M W_M (1 - \nu_{PDMS}^2)}{m^2 n^2 \pi^4 E_{PDMS} H_M^3 [(m\pi/L_M)^2 + (n\pi/W_M)^2]^2} \quad (2)$$

where L_M , W_M and H_M are the membrane length, width and thickness, E_{PDMS} [=750 kPa (Armani et al. 1999)] is the

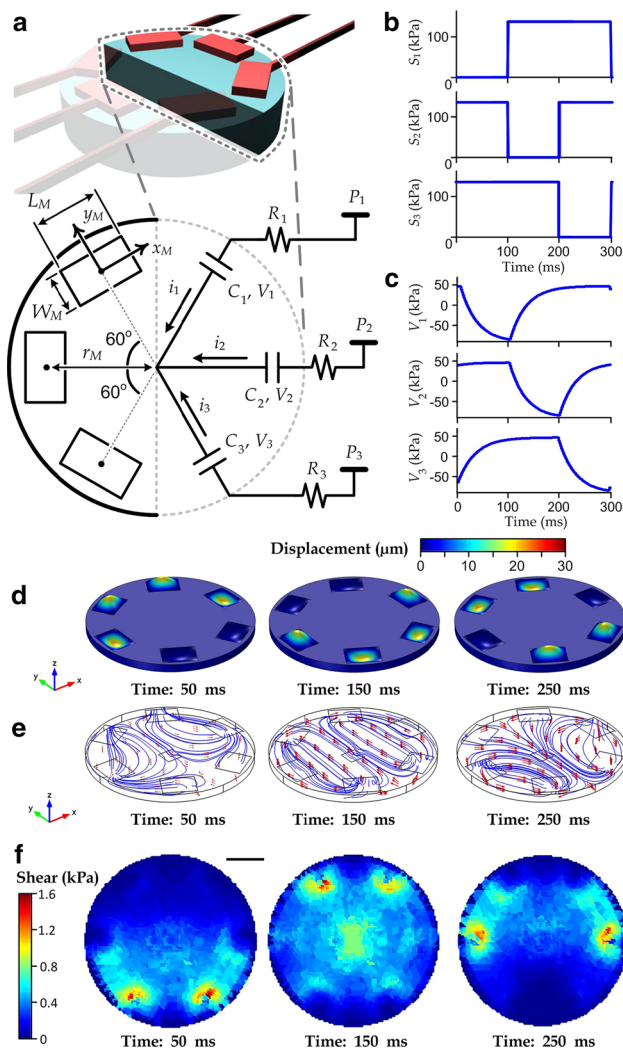


Fig. 2 Simulation of flows in a mixing micro-chamber model. **a** Lumped-element circuit model representing membrane dynamics of the half-chamber model. We considered the membrane configurations defined by membrane-center to chamber-center distance (r_M), membrane length (L_M) and width (W_M). **b** Pressure inputs from inlets of the control channels for micro-mixer design model I. **c** Simulated pressure differences across the membranes. Profiles of **d** membrane deflections, **e** flow velocities and **f** shear stress over the chamber base of model I, at time 50, 150 and 250 ms in a stabilized mixing cycle

Young’s modulus of PDMS and ν_{PDMS} (≈ 0.5) is the Poisson’s ratio of PDMS, respectively.

We defined the liquid flow rates along control channels as the electrical currents (i_1 , i_2 and i_3), the driving pressure at the control channel inlets as the input voltages (S_1 , S_2 and S_3) and the pressure differences across the membranes as voltages (V_1 , V_2 and V_3). During the mixing operations, the chamber was isolated (without net inflow and outflow) and the fluidic resistance of the chamber should be negligible,

compared to the resistances of the control channels. We expressed this effect by linking the membrane capacitors at a common node following the *Kirchhoff’s* current law. We then obtained the following relations:

$$S_1 - S_3 = i_1 R_1 + V_1 - V_3 - i_3 R_3$$

$$S_2 - S_3 = i_2 R_2 + V_2 - V_3 - i_3 R_3$$

$$C_j \dot{V}_j = i_j, \quad \text{for } j = 1, 2 \text{ and } 3$$

$$i_1 + i_2 + i_3 = 0 \tag{3}$$

Alternatively, we could write all these relations as a linear system in the state-space form:

$$\begin{bmatrix} C_1 & 0 & -R_3 C_3 / R_1 \\ 0 & C_2 & -R_3 C_3 / R_2 \\ C_1 & C_2 & C_3 \end{bmatrix} \begin{bmatrix} \dot{V}_1 \\ \dot{V}_2 \\ \dot{V}_3 \end{bmatrix} = \begin{bmatrix} -1/R_1 & 0 & 1/R_1 \\ 0 & -1/R_2 & 1/R_2 \\ 0 & 0 & 0 \end{bmatrix} \begin{bmatrix} V_1 \\ V_2 \\ V_3 \end{bmatrix} + \begin{bmatrix} 1/R_1 & 0 & -1/R_1 \\ 0 & 1/R_2 & -1/R_2 \\ 0 & 0 & 0 \end{bmatrix} \begin{bmatrix} S_1 \\ S_2 \\ S_3 \end{bmatrix} \tag{4}$$

We defined S_1 , S_2 and S_3 as functions of time, during one mixing cycle (300 ms) were in the form as plotted in Fig. 2b, including the switching of membrane pressurization every 100 ms. The driving pressures at the actuation states were set at a consistent level (~ 137.9 kPa), matching with the experiment configurations. We then computed for the corresponding stabilized one-cycle transient responses of the half-chamber mixer model to obtain the transient V_1 , V_2 and V_3 , as functions of time. In practice, we obtained the stabilized responses (Fig. 2c) by simulating 20 mixing cycles with zero initial conditions and extracted only the last-cycle response.

V_1 , V_2 and V_3 were then converted to spatial deflections of the membranes (Θ_1 , Θ_2 and Θ_3) in the local membrane coordinate frames with local origins at the membrane centers as described in Fig. 2a:

$$\Theta_j(x, y) = \sum_{m=1,3,\dots} \sum_{n=1,3,\dots} \frac{192(1 - \nu_{PDMS}^2) \sin(m\pi x/W_M) \sin(n\pi y/L_M)}{m n \pi^2 E_{PDMS} H_M^3 [(m\pi/L_M)^2 + (n\pi/W_M)^2]^2} \times V_j \quad \text{for } j = 1, 2 \text{ and } 3; \quad -L_M/2 < x < L_M/2; \quad \text{and } -W_M/2 < y < W_M/2. \tag{5}$$

Θ_1 , Θ_2 and Θ_3 should be reasonable approximations as long as the membranes do not contact with the chamber base at any time during the mixing cycle. For this reason, we chose S_1 , S_2 and S_3 at a sufficiently low level, i.e., 137.9 kPa.

3.3 Flow characteristics

We used commercial simulation software (COMSOL 4.3b, COMSOL Inc., Burlington, MA, USA) to perform simulations of flows in a chamber under moving boundaries calculated by the lump model. We first considered a template mixing design with the membrane dimensions: $r_M = 400 \mu\text{m}$, $L_M = 200 \mu\text{m}$, $W_M = 150 \mu\text{m}$ and $H_M = 20 \mu\text{m}$. However, both the simulation and experiment studies have shown that this design could not induce significant mixing performance (data not shown). Based on this template design, we considered two modifications of the membrane dimensions by either reducing the membrane thickness (model I: $r_M = 400 \mu\text{m}$, $L_M = 200 \mu\text{m}$, $W_M = 150 \mu\text{m}$ and $H_M = 10 \mu\text{m}$) or enlarging the membrane areas (model II: $r_M = 360 \mu\text{m}$, $L_M = 230 \mu\text{m}$ and $W_M = 220 \mu\text{m}$ and $H_M = 20 \mu\text{m}$), in order to reduce the membrane stiffness. The simulated profiles of membrane displacements, flow velocities and shear stress over the chamber base of model I are shown in Fig. 2d–f, whereas the profiles for model II are available in Fig. S2. Because the generated circulating liquid flows (average velocity for model I: $0.363 \times 10^3 \mu\text{m/s}$ and average velocity for model II: $0.178 \times 10^3 \mu\text{m/s}$) were sufficiently slow, the *Reynolds* numbers were $\sim 10^{-20}$ and the corresponding acoustic *Reynolds* numbers (Friend and Yeo 2011; Sayar and Farouk 2011, 2012, 2015; Yeo and Friend 2009) were also very small ($\ll 1$). Notably, fluctuations in hydraulic pressure in the chamber ($< 10 \text{ Pa}$ for both models) were much smaller than the changes of driving pressures (137.9 kPa) because the pressure drops happened mainly in the control channels (R_1 , R_2 and R_3). These pressure fluctuations induced only negligible further deflections of C_1 , C_2 and C_3 . Additionally, the maximum membrane downward deflections were 29.6 and 38.6 μm for model I and model II, respectively. This double confirmed that there was no mechanical contact between the membranes and the chamber base. Further, we have calculated also the shear stress over the bottom surface of the micro-chamber $\tau(x, y, t)|_{z=0}$:

$$\begin{aligned} \tau(x, y, t)|_{z=0} &= \mu \left. \frac{\partial (\sqrt{u^2 + v^2})}{\partial z} \right|_{z=0} \\ &\approx \mu \left(\frac{\sqrt{u(x, y, \Delta z, t)^2 + v(x, y, \Delta z, t)^2}}{\Delta z} \right) \end{aligned} \quad (6)$$

where u and v are the local velocity components along x - and y -directions, respectively. We chose $\Delta z = 1 \mu\text{m}$ such that Δz is sufficiently small for a reasonable approximation. Results (Fig. 2f) show that the maximum shear stresses (model I: $\sim 0.173 \text{ kPa}$ and model II: $\sim 0.102 \text{ kPa}$) should not cause any harmful effects on the cell viability

(Lange et al. 2001; Legazpi et al. 2009; Scragg et al. 1988; Shiragami and Unno 1994) and shear-induced movements (Hyon et al. 2012; Koh and Marcos 2015; Marcos et al. 2009, 2011, 2012, 2014; Marcos and Stocker 2006).

3.4 Mixing of soluble substances

We performed simulations by COMSOL 4.3b, with the convection–diffusion equations as the governing equations in the chamber model. We assumed the liquid diffusivity was close to pure water ($\sim 10^{-9} \text{ m}^2/\text{s}$). To reduce the computation complexity, we decoupled the simulation into two stages: (1) liquid flows induced by the membrane movements and (2) transient concentration profiles under the flow. We adopted only the stabilized velocity profile because the flow stabilization took $< 2 \text{ s}$ (a few mixing cycles), which was negligible comparing to the entire mixing duration ($\geq 30 \text{ s}$). The velocity profile at time t should be equal to the extracted stabilized velocity profile at t_s with the relation $t = 0.3 N + t_s$, where N is the number of previous mixing cycles.

We further compared the results between the simulations and the experiments. To facilitate the comparison, we converted the 3D simulation results into spatial 2D profiles, by averaging concentrations along the vertical (z) direction at different ‘top-view’ positions (i.e., x and y). We quantified the simplified concentration profiles using standard deviations over the chamber top views, $\text{SD}(t)$, at different mixing time t . We normalized $\text{SD}(t)$ as $\text{SD}'(t) = [\text{SD}(t) - \text{SD}(t \rightarrow \infty)] / [\text{SD}(0) - \text{SD}(t \rightarrow \infty)]$, such that SD' equals ‘1’ at the beginning and drops toward ‘0’ throughout mixing (Voth et al. 2003). We defined the ‘mixing time’ as the moment where SD' drops to ‘0.1’ to characterize the mixing performance.

Additionally, we conducted experiments to characterize SD' and the mixing time under different values of the membrane switching time. Results show reasonable agreements between simulations and experiments, for mixing time in the cases without mixing (simulation: 157 s; experiment: 179 s. Fig. 3a), model I (simulation: 87 s; experiment: 67 s. Fig. S3) and model II (simulation: 30 s; experiment: 43 s. Fig. 3b). Due to the better mixing performance, we adopted the mixer model II as our model device for the following analyses. As shown in Fig. 3c, the optimal switching time for shortest mixing time of soluble substances was $\sim 100 \text{ ms}$ for model II.

3.5 Mixing of particles

Experiments were also conducted for the mixing of microparticles driven by the microfluidic mixer for different pumping switching times. The selected fluorescent beads (Cat# FP-0545-2, carboxyl fluorescent light yellow

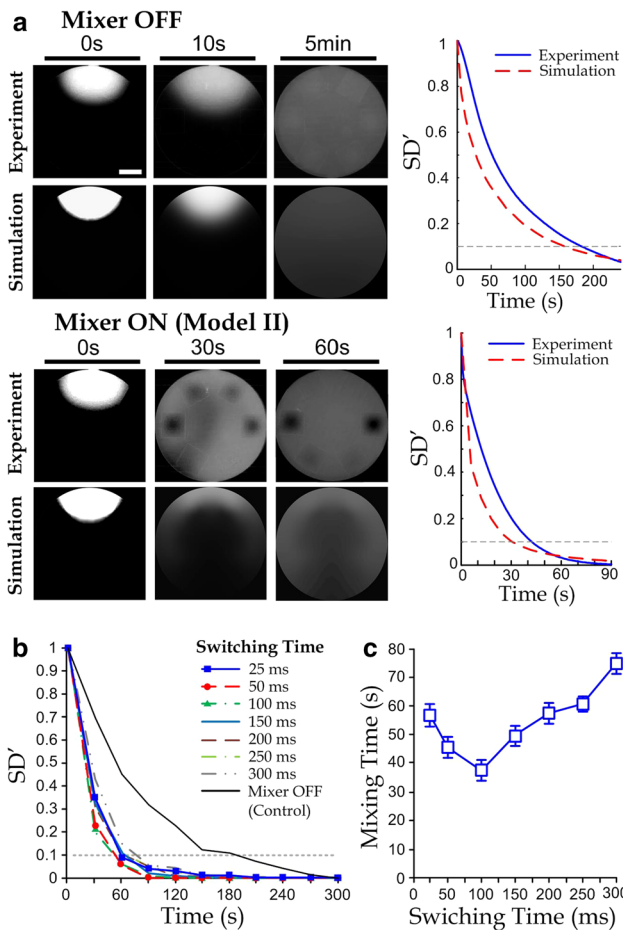


Fig. 3 Mixing of color dyes. **a** Examples of simulation and experimental intensity profiles. Comparison between pure diffusion (*upper*) and mixing of the mixer design model II with a membrane switching time of 100 ms (*lower*, results for model I are shown in Fig. S3). Experimental results for mixer model II under different membrane switching time intervals: **b** averaged transient normalized standard deviation (SD') and **c** mixing time [number of repeating experiments (N): >20]. Error bars represent standard deviations of the mixing time

particles, Spherotech, Inc., Lake Forest, IL) had a comparable size (diameter: ~500 nm) with some bacteria (e.g., *Escherichia coli* and *S. mutans*); therefore, these results of the fluorescent beads should be, to certain extent, representative to mixing of the bacteria.

On the other hand, computation of the particle tracing was implemented to investigate the mixing for sub-microscale particles (e.g., bacteria and fluorescent micro-beads). We applied the previously computed transient velocity profiles and performed the particle simulation for one mixing cycle (duration: 300 ms) in COMSOL. In this simulation, a particle was released from each node of the mesh model of the chamber. The final positions (time: 300 ms) of all particles were then exported and stored. Owing to the cyclic membrane movements during the mixing operation,

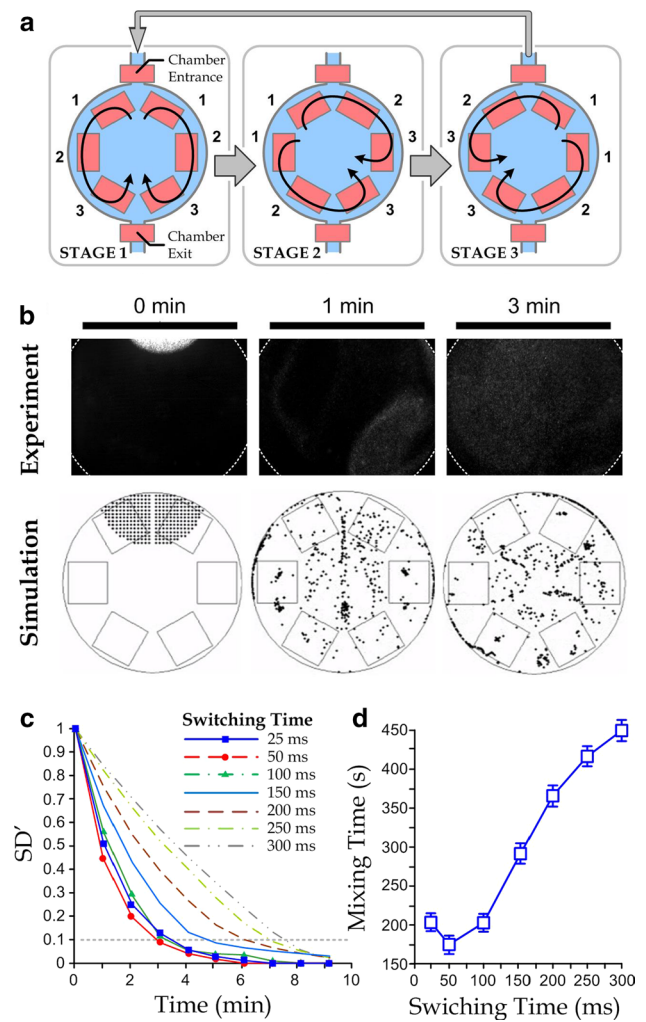


Fig. 4 **a** Three repeating stages of mixing with different membrane groupings for switching flow directions. **b** Mixing results of fluorescent beads implemented by the device model II. Dotted lines are the chamber boundaries. **c** Averaged SD' at different time points under different switching time intervals. **d** Mixing time as a function of the switching time interval ($N > 20$). Error bars represent standard deviation of data points

the chamber geometry should restore at the end of every mixing cycle. Therefore, we may neglect the membrane dynamics within the cycle by considering only the particle dislocations for every time step of the mixing duration (300 ms). For the particle tracking over a longer period, we have developed a customized MATLAB script to compute the particle trajectories with a time step of 300 ms. The particle dislocations inside each grid volume were approximated by the trilinear interpolation scheme using the nodal values of the enclosing grid. Both the simulation and experimental results (Fig. S4) revealed that two chamber regions were ineffective for the particle mixing.

To solve the mentioned limited mixing problem, we extended the mixing operation by implementing a mixing

mode with repeatedly changing grouping of the six membranes as shown in Fig. 4b. Three stages of the membrane grouping were switched every 12 s, in order to generate circulation flows to enhance mixing in different directions. The simulation and experimental results (Fig. 4c) have demonstrated that the extended operations can induce an even distribution of the mixed particle profile.

Analogous to the analyses for the soluble substances, we performed repeated experiments (at least 20 trials for each switching time interval) to further investigate the transient SD' for different switching time (Fig. 4d) and the mixing time as a function of the switching time (Fig. 4e). Results show that the particle mixing should operate with a switching time interval ~ 50 ms for the more efficient mixing. Indeed, the extended operation can be used also for the soluble substances to ensure a thorough mixing.

3.6 Experimental verification with cell culture

Cell culture experiments were further conducted to demonstrate the improvements of cell growth consistency and viability in the long term. The dental bacterium *S. mutans* was selected here. In particular, the *S. mutans* species is well known of its key role in the early development of human dental biofilms (Loesche 1986). The attachment of *S. mutans* on the tooth/pellicle substrates in human oral cavity forms a firm foundation for the following cell–cell adhesion between *S. mutans* and other bacteria (e.g., *Fusobacterium nucleatum*) involved in the later development of mature dental biofilm. Therefore, the culture of an evenly distributed layer of *S. mutans* can be further applied to the quantitative study of early dental biofilm formation and the corresponding mechanisms.

In our experiments, *S. mutans* cells were injected into the micro-mixer chamber following the procedures described in “Methods” and subsequently maintained under the microenvironment under the ambient gas condition, ~ 37 °C temperature and a regular injection of fresh culture media. Considering that the overall salivary flow rate in human oral cavity (volume: ~ 100 ml) is ~ 0.22 ml/min (Watanabe and Dawes 1990), we have set the average medium flow rate in the micro-chamber (capacity: ~ 62.8 pl) at ~ 0.363 pl/min for a reasonable liquid velocity. Furthermore, the flow rate of the medium injection operation was set as ~ 30 pl/min for 30 s once every 30 min, corresponding to average flow rate 0.5 pL/min and a maximum shear over the chamber base of ~ 0.02 Pa. On the other hand, we applied the device configuration ‘model II’ for the more effective mixing (switching time: 100 ms; driving pressure: 137.9 kPa) and the mixing operation was applied for 3 min after every medium injection.

An experiment was performed to show that *S. mutans* would grow faster near the chamber inlet for the medium

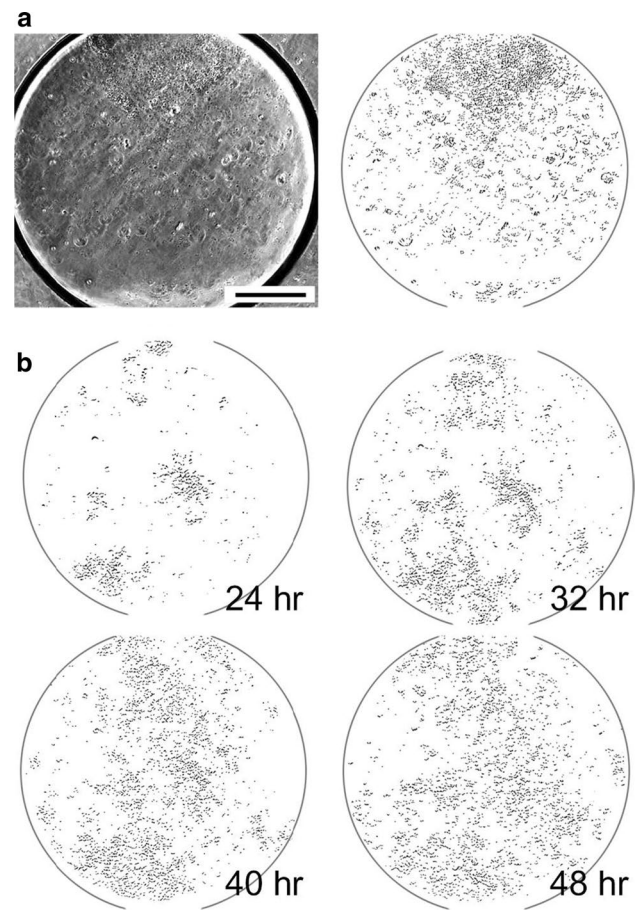


Fig. 5 **a** Phase-contrast microscopic image (left; scale bar: 200 μ m) and image-processed distribution (right) of *S. mutans* population in a micro-chamber without assist of the mixing for a cultivation duration of 48 h. The upper side is the chamber inlet region. The gray circle indicates the chamber boundary. **b** Image-processed profiles of the *S. mutans* population growing in a micro-chamber at different time points (24, 32, 40 and 48 h) with the mixing operations applied regularly over time (the corresponding microscopic images are available in Fig. S5)

injection without the peristaltic mixing operation (Fig. 5a). We analyzed the phase-contrast microscopic images of the cell distribution in the micro-chamber using an image processing scheme as reported in our previous works (Cui et al. 2014; Lam et al. 2009). Briefly, the background pattern of chamber region was estimated by the convolution of the image with a Gaussian mask (size: 20 pixel \times 20 pixel, radius: 10 pixel) as a low-pass image filter. After subtracting the image intensities by the filtered background, the bacteria region would then be shown as darker patterns. Thresholding was then performed identify bacterial cells (black) as shown in Fig. 5a (right).

Furthermore, culture experiments of *S. mutans* were also applied with the medium injection and mixing operations. As an example, time-lapsed images of the *S. mutans* population (at 24, 32, 40 and 48 h) show the cells grew with

an even distribution, induced by the mixing operation of freshly injected media (Fig. 5b). This result indicates that the peristaltic mixing scheme is effective to generate a more consistent microenvironment for even cell growth and to avoid cell clogging at chamber inlet.

4 Conclusion

In this study, a microfluidic mixer operating inside an enclosed micro-chamber was reported on the device design, function optimization and cell culture application. This mixer consisted of six microscale PDMS membranes, which were paired up as two peristaltic flow drivers. Circulation flows were induced based on the membrane movements (driven by external compressed-air pressures applied in a peristaltic manner) over the chamber boundaries. We have characterized multiple device configurations and demonstrated that the membrane parameters $r_M = 360 \mu\text{m}$, $L_M = 230 \mu\text{m}$ and $W_M = 220 \mu\text{m}$ and $H_M = 20 \mu\text{m}$ can induce an effective mixing. Further, we introduced an extended mixing operation by changing grouping of the membranes for driving the circulation flows in different directions repeatedly. Quantitative analyses on the transient concentration profiles of color dyes and fluorescent beads have shown that the mixing can be optimized with the switching time of 100 and 50 ms for soluble substances and microparticles, respectively. As the comparable diameters between the fluorescent beads and the bacteria, the optimized operations for beads were further applied for the culture of bacteria with the equivalent diameters. We applied the mixing scheme to the culture of *S. mutans* to achieve a more evenly distributed bacteria clusters during their growth up to 2 days. The improvement on the growth consistency of *S. mutans* in the micro-chamber is obvious, comparing to the control case (no mixing) that the cell growth accumulated near the chamber inlet. In essence, this work has demonstrated the effectiveness and applicability of the microfluidic peristaltic mixing scheme based on moving boundaries of the chambers, driven by six deformable micro-membranes. As the soft lithography-based fabrication enables the direct integration of the multiple micro-mixers in microfluidics, this work can induce improvements and extended applications of microfluidics such as biomedical diagnosis and high-throughput bio-sample processing.

Acknowledgments We sincerely thank for the supports during the early development of this research from Department of Mechanical Engineering in Massachusetts Institute of Technology. We appreciate the invaluable advices from Dr. T. Thorsen. We thank for the financial supports from City University of Hong Kong (Seed Grant; project #7003019), Croucher Foundation Scholarship and General Research Grant of Hong Kong Research Grant Council (project# RGC115813).

References

- Abbas Y, Miwa J, Zengerle R, von Stetten F (2013) Active continuous-flow micromixer using an external braille pin actuator array. *Micromachines* 4:80–89
- Materne E-M et al (2013) Dynamic culture of human liver equivalents inside a micro-bioreactor for long-term substance testing. In: *BMC Proceedings of BioMed Central Ltd. Suppl* 6:P72
- Ansari MA, Kim K-Y, Anwar K, Kim SM (2010) A novel passive micromixer based on unbalanced splits and collisions of fluid streams. *J Micromech Microeng* 20:055007
- Armani D, Liu C, Aluru N (1999) Re-configurable fluid circuits by PDMS elastomer micromachining. In: *Twelfth IEEE International Conference on Micro Electro Mechanical Systems, 1999. MEMS'99, Ieee*, pp 222–227
- Byus CV, Pieper SE, Adey WR (1987) The effects of low-energy 60-Hz environmental electromagnetic fields upon the growth-related enzyme ornithine decarboxylase. *Carcinogenesis* 8:1385–1389
- Capretto L, Cheng W, Hill M, Zhang X (2011) *Micromixing within microfluidic devices*. Springer, New York, pp 27–68
- Cui X, Yip HM, Zhu Q, Yang C, Lam RHW (2014) Microfluidic long-term differential oxygenation for bacterial growth characteristics analyses. *RSC Adv* 4:16662–16673. doi:10.1039/C4RA01577K
- Friend J, Yeo LY (2011) Microscale acoustofluidics: microfluidics driven via acoustics and ultrasonics. *Rev Mod Phys* 83:647
- Fu L-M, Ju W-J, Tsai C-H, Hou H-H, Yang R-J, Wang Y-N (2013) Chaotic vortex micromixer utilizing gas pressure driving force. *Chem Eng J* 214:1–7
- Fu L-M, Fang W-C, Hou H-H, Wang Y-N, Hong T-F (2014) Rapid vortex microfluidic mixer utilizing double-heart chamber. *Chem Eng J* 249:246–251
- Hsiung S-K, Lee C-H, Lin J-L, Lee G-B (2007) Active micro-mixers utilizing moving wall structures activated pneumatically by buried side chambers. *J Micromech Microeng* 17:129
- Hyon Y, Marcos, Powers TR, Stocker R, Fu HC (2012) The wiggling trajectories of bacteria. *J Fluid Mech* 705:58–76
- Jang L-S, Chao S-H, Holl MR, Meldrum DR (2007) Resonant mode-hopping micromixing. *Sens Actuators A Phys* 138:179–186
- Kim S-J, Wang F, Burns MA, Kurabayashi K (2009) Temperature-programmed natural convection for micromixing and biochemical reaction in a single microfluidic chamber. *Anal Chem* 81:4510–4516
- Koh JBY, Marcos (2015) The study of spermatozoa and sorting in relation to human reproduction. *Microfluid Nanofluid* pp. 1–20
- Lam RHW, Kim M-C, Thorsen T (2009) Culturing aerobic and anaerobic bacteria and mammalian cells with a microfluidic differential oxygenator. *Anal Chem* 81:5918–5924. doi:10.1021/ac9006864
- Lange H, Taillandier P, Riba JP (2001) Effect of high shear stress on microbial viability. *J Chem Technol Biotechnol* 76:501–505
- Lee C-Y, Chang C-L, Wang Y-N, Fu L-M (2011a) Microfluidic mixing: a review. *Int J Mol Sci* 12:3263–3287
- Lee KS, Boccazzi P, Sinsky AJ, Ram RJ (2011b) Microfluidic chemostat and turbidostat with flow rate, oxygen, and temperature control for dynamic continuous culture. *Lab Chip* 11:1730–1739
- Legazpi L, Laca A, Díaz M (2009) Kinetic analysis of hybridoma cells viability under mechanical shear stress with and without serum protection. *Bioprocess Biosyst Eng* 32:717–722
- Lin C-H, Tsai C-H, Pan C-W, Fu L-M (2007) Rapid circular microfluidic mixer utilizing unbalanced driving force. *Biomed Microdevices* 9:43–50
- Lin Y-H, Wang C-C, Lei KF (2014) Bubble-driven mixer integrated with a microfluidic bead-based ELISA for rapid bladder cancer biomarker detection. *Biomed Microdevices* 16:199–207

- Liu RH, Yang J, Pindera MZ, Athavale M, Grodzinski P (2002) Bubble-induced acoustic micromixing. *Lab Chip* 2:151–157
- Loesche WJ (1986) Role of *Streptococcus mutans* in human dental decay. *Microbiol Rev* 50:353–380
- Mansur EA, Ye M, Wang Y, Dai Y (2008) A state-of-the-art review of mixing in microfluidic mixers. *Chin J Chem Eng* 16:503–516
- Marcos, Stocker R (2006) Microorganisms in vortices: a microfluidic setup. *Limnol Oceanogr Methods* 4:392–398
- Marcos, Fu HC, Powers TR, Stocker R (2009) Separation of micro-scale chiral objects by shear flow. *Phys Rev Lett* 102:158103
- Marcos, Seymour JR, Luhar M, Durham WM, Mitchell JG, Macke A, Stocker R (2011) Microbial alignment in flow changes ocean light climate. *Proc Natl Acad Sci* 108:3860–3864
- Marcos, Fu HC, Powers TR, Stocker R (2012) Bacterial rheotaxis. *Proc Natl Acad Sci* 109:4780–4785
- Marcos, Tran NP, Saini AR, Ong KCH, Chia WJ (2014) Analysis of a swimming sperm in a shear flow. *Microfluid Nanofluid* 17:809–819
- Nguyen N-T, Wu Z (2005) Micromixers—a review. *J Micromech Microeng* 15:R1
- Park C, Wereley ST (2013) Rapid generation and manipulation of microfluidic vortex flows induced by AC electrokinetics with optical illumination. *Lab Chip* 13:1289–1294
- Peng Z-C, Hesketh P, Mao W, Alexeev A, Lam W (2011) A microfluidic mixer based on parallel, high-speed circular motion of individual microbeads in a rotating magnetic field. In: *Solid-State Sensors, Actuators and Microsystems Conference (TRANSDUCERS)*, 16th International, 2011. IEEE, pp 1292–1295
- Pitt WG, Ross SA (2003) Ultrasound increases the rate of bacterial cell growth. *Biotechnol Prog* 19:1038–1044
- Sayar E, Farouk B (2011) Acoustically generated flows in microchannel flexural plate wave sensors: effects of compressibility. *Sens Actuators A Phys* 171:317–323
- Sayar E, Farouk B (2012) Multifield analysis of a piezoelectric valveless micropump: effects of actuation frequency and electric potential. *Smart Mater Struct* 21:075002
- Sayar E, Farouk B (2015) Bulk acoustic wave piezoelectric micropumps with stationary flow rectifiers: a three-dimensional structural/fluid dynamic investigation. *Microfluid Nanofluid* pp. 1–13
- Scragg A, Allan E, Leckie F (1988) Effect of shear on the viability of plant cell suspensions. *Enzyme Microb Technol* 10:361–367
- Senturia SD (2001) *Microsystem design*, vol 3. Kluwer Academic Publishers, Boston
- Shiragami N, Unno H (1994) Effect of shear stress on activity of cellular enzyme in animal cell. *Bioprocess Eng* 10:43–45
- Timoshenko S, Woinowsky-Krieger S, Woinowsky-Krieger S (1959) *Theory of plates and shells*, vol 2. McGraw-hill, New York
- Tofteberg T, Skolimowski M, Andreassen E, Geschke O (2010) A novel passive micromixer: lamination in a planar channel system. *Microfluid Nanofluid* 8:209–215
- Unger MA, Chou H-P, Thorsen T, Scherer A, Quake SR (2000) Monolithic microfabricated valves and pumps by multilayer soft lithography. *Science* 288:113–116
- Vianale G, Reale M, Amerio P, Stefanachi M, Di Luzio S, Muraro R (2008) Extremely low frequency electromagnetic field enhances human keratinocyte cell growth and decreases proinflammatory chemokine production. *Br J Dermatol* 158:1189–1196
- Voth GA, Saint T, Dobler G, Gollub JP (2003) Mixing rates and symmetry breaking in two-dimensional chaotic flow. *Phys Fluids* (1994-present) 15:2560–2566
- Watanabe S, Dawes C (1990) Salivary flow rates and salivary film thickness in five-year-old children. *J Dent Res* 69:1150–1153
- West J et al (2002) Application of magnetohydrodynamic actuation to continuous flow chemistry. *Lab Chip* 2:224–230
- Wu M-H, Huang S-B, Cui Z, Cui Z, Lee G-B (2008) Development of perfusion-based micro 3-D cell culture platform and its application for high throughput drug testing. *Sens Actuators B Chem* 129:231–240
- Xia H, Seah Y, Liu Y, Wang W, Toh AG, Wang Z (2014) Anti-solvent precipitation of solid lipid nanoparticles using a microfluidic oscillator mixer. *Microfluid Nanofluid* pp. 1–8
- Yan D, Yang C, Miao J, Lam Y, Huang X (2009) Enhancement of electrokinetically driven microfluidic T-mixer using frequency modulated electric field and channel geometry effects. *Electrophoresis* 30:3144–3152
- Yeo LY, Friend JR (2009) Ultrafast microfluidics using surface acoustic waves. *Biomicrofluidics* 3:012002
- Zhu X, Kim ES (1998) Microfluidic motion generation with acoustic waves. *Sens Actuators A Phys* 66:355–360